Volume 902 1 January 2016 ISSN 0003-2670

ELSEVIER

# ANALYTICA CHIMICA ACTA

AN INTERNATIONAL JOURNAL DEVOTED TO ALL BRANCHES OF ANALYTICAL CHEMISTRY

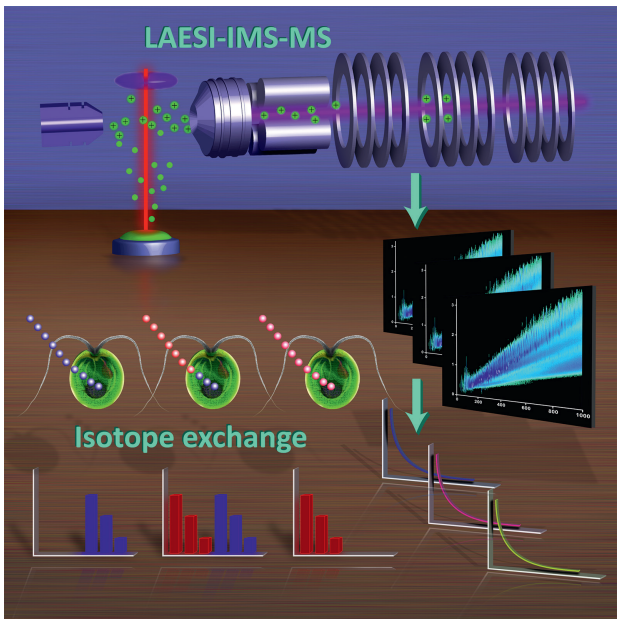




## Featured Article

Turnover rates in microorganisms by laser ablation electrospray ionization mass spectrometry and pulse-chase analysis

Sylwia A. Stopka, Tarek R. Mansour, Bindesh Shrestha, Eric Marechal, Denis Falconet, Akos Vertes

*(Published in pages 1–7 of this issue)*

Analytica Chimica Acta 902 (2016) 1–7

Contents lists available at ScienceDirect

Analytica Chimica Acta

journal homepage: www.elsevier.com/locate/aca

# Turnover rates in microorganisms by laser ablation electrospray ionization mass spectrometry and pulse-chase analysis

Sylwia A. Stopka[a], Tarek R. Mansour[a], Bindesh Shrestha[a], Éric Maréchal[b], Denis Falconet[b], Akos Vertes[a,*]

[a] Department of Chemistry, W.M. Keck Institute for Proteomics Technology and Applications, The George Washington University, Washington, DC 20052, USA
[b] Laboratoire de Physiologie Cellulaire et Végétale, UMR 5168, CEA-CNRS-INRA-Univ. Grenoble Alpes, Grenoble, France

## HIGHLIGHTS

- High-throughput pulse-chase analysis using direct sampling of biological cells.
- Ion mobility separation for the elucidation of isotopologs.
- Identification of isotopologs in difference heat plots of DT vs. *m*/*z*.
- Simultaneous determination of turnover rates for lipids and peptides in microalgae.

## GRAPHICAL ABSTRACT

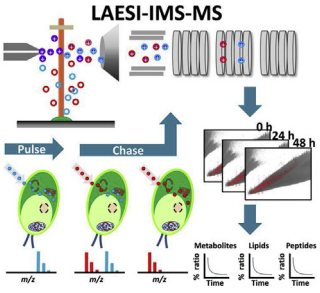


## ARTICLE INFO

*Article history:*
Received 2 June 2015
Received in revised form 20 August 2015
Accepted 23 August 2015
Available online 1 September 2015

*Keywords:*
Turnover rate
Cell
Mass spectrometry
Pulse-chase analysis
Laser ablation electrospray ionization

## ABSTRACT

Biochemical processes rely on elaborate networks containing thousands of compounds participating in thousands of reaction. Rapid turnover of diverse metabolites and lipids in an organism is an essential part of homeostasis. It affects energy production and storage, two important processes utilized in bioengineering. Conventional approaches to simultaneously quantify a large number of turnover rates in biological systems are currently not feasible. Here we show that pulse-chase analysis followed by laser ablation electrospray ionization mass spectrometry (LAESI-MS) enable the simultaneous and rapid determination of metabolic turnover rates. The incorporation of ion mobility separation (IMS) allowed an additional dimension of analysis, i.e., the detection and identification of isotopologs based on their collision cross sections. We demonstrated these capabilities by determining metabolite, lipid, and peptide turnover in the photosynthetic green algae, *Chlamydomonas reinhardtii*, in the presence of $^{15}$N-labeled ammonium chloride as the main nitrogen source. Following the reversal of isotope patterns in the chase phase by LAESI-IMS-MS revealed the turnover rates and half-lives for biochemical species with a wide range of natural concentrations, e.g., chlorophyll metabolites, lipids, and peptides. For example, the half-lives of lyso-DGTS(16:0) and DGTS(18:3/16:0), $t_{1/2}$ = 43.6 ± 4.5 h and 47.6 ± 2.2 h, respectively, provided insight into lipid synthesis and degradation in this organism. Within the same experiment, half-lives for chlorophyll *a*, $t_{1/2}$ = 24.1 ± 2.2 h, and a 2.8 kDa peptide, $t_{1/2}$ = 10.4 ± 3.6 h, were also determined.



http://dx.doi.org/10.1016/j.aca.2015.08.047
0003-2670/

## 1. Introduction

Metabolic network reconstructions with thousands of metabolites and reactions exhibit remarkable complexity. For example, the iRC1080 reconstruction of the *Chlamydomonas reinhardtii* pathways accounts for 1068 metabolites and 2190 reactions in 10 cellular compartments [1]. Understanding the homeostasis of organisms, based on a robust regulation of these networks, requires detailed information on the turnover of many biochemical species. The main factors defining turnover are the existing pools of molecules and the net sum of the incoming and outgoing fluxes.

Over the years stable isotope labeling has been incorporated in metabolic studies to improve metabolite identification, perform quantification, and obtain reaction kinetics information for biochemical pathways [2]. Dynamic changes in labeled chemical species in metabolic networks are most often followed by mass spectrometry. Monitoring the propagation of isotope labeling through the metabolic network in combination with perturbations, e.g., genetic knockouts or a drug treatment, on well-known pathways, such as the central carbon metabolism (tricarboxylic acid cycle, glycolysis, and pentose phosphate pathway), provide information on metabolic fluxes in health and disease [3]. New metabolic networks and connections can be mapped by monitoring the incorporation of the labels [4]. Other applications of pathway analysis and genetic manipulation include metabolic engineering to promote the production of high value chemicals by microorganisms [5,6].

Stable isotope labeling of amino acids in cell cultures (SILAC), where $^{13}$C-labeled essential amino acids are incorporated in the medium, is predominantly used for labeling of metabolites in mammalian cells [7]. A similar approach can be applied to label plant cells, where salts and/or sugars containing $^{13}$C or $^{15}$N isotopes can be incorporated in the media [8–10]. This technique has been applied in model systems including *Saccharomyces cerevisiae*, *Caenorhabditis elegans*, *Arabidopsis thaliana*, and *C. reinhardtii* [11–13].

Pulse-chase analysis consists of two phases [14]. In the pulse phase, cells are cultured in a labeled medium, whereas in the chase phase, the medium is reverted to the unlabeled form. During the latter phase, the time dependence of isotopolog composition is determined by mass spectrometry (MS). Due to its high sensitivity and wide dynamic range, MS in combination with chromatographic separation methods is increasingly used for turnover measurements [15]. Powerful methods, e.g., GC–MS with stable isotope labeling, exist for the simultaneous determination of multiple metabolite fluxes in microbial systems [16–18]. However, due to the long retention times, time consuming extraction, hydrolysis and derivatization protocols in conventional separations, and the large quantity of species required to be labeled, result in low throughput.

The ambient ionization technique, laser ablation electrospray ionization (LAESI) MS, has been used for the rapid detection and identification of diverse metabolites, lipids, and peptides [19]. Recently coupling ion mobility separation (IMS) to this platform allowed for the high-throughput elucidation of lipids and metabolites in microalgae [20,21]. The analysis time is reduced from the typical ~20 min needed for HPLC to ~200 ms required for an IMS separation.

To demonstrate the utility of this method, *C. reinhardtii* was selected because this photosynthetic organism has a well-studied lipid metabolism [22,23] and has the ability to produce substantial amounts of lipids, which in turn can be processed into biofuels [14]. Using $^{13}$C-based methods, e.g., SILAC, would result in reduced levels of labeling (~80%) because *C. reinhardtii* is autotrophic [24–27]. To achieve higher isotope incorporation for molecules containing nitrogen, $^{15}$N-ammonium chloride is used in the culture [28]. In this contribution, the first combination of pulse-chase analysis with the LAESI-IMS-MS technique allows for high throughput determination of turnover rates with extensive metabolite and lipid coverage.

## 2. Experimental

### 2.1. Chemicals

The 99% enriched [$^{15}$N]-ammonium chloride was purchased from Cambridge Isotope (Andover, MA). Original Hutner's Trace element stock was obtained from the Chlamydomonas Resource Center at the University of Minnesota. Chlorophyll *a* standard was purchased from Sigma–Aldrich (St. Louis, MO). The 50% methanol electrospray solution contained 0.1% acetic acid that was purchased as glacial acetic acid (≥99.0%) from Fluka (St. Louis, MO). Certified HPLC grade methanol and water were obtained from Alfa Aesar (Ward Hill, MA).

### 2.2. Growth media

Two types of tris acetate phosphate (TAP) media [29] were made in house, unlabeled containing natural nitrogen isotope distribution and $^{15}$N-labled produced by using 99% enriched $^{15}$N-labeled ammonium chloride. Both media contained the following components: 2.42 g of tris base, 25.0 mL of Beijerinck salts, 1.0 mL phosphate solution, 1.0 mL Hutner trace element solution, and 1.0 mL glacial acetic acid. The final concentrations were 7 mM $NH_4Cl$, 830 μM $MgSO_4$, and 450 μM $CaCl_2$ for the Beijerinck salts and 1.65 mM $K_2HPO_4$ and 1.05 mM $KH_2PO_4$ for the phosphate solution. The pH values of the media were adjusted to 7.0, and the TAP solutions were diluted to 1000 mL by water. The resulting solutions were autoclaved (Hiclave HVA-85, Hirayama, Concord, CA) at 121 °C for 20 min and stored at 4 °C in a dark environment.

### 2.3. Cell culture

Wild type *C. reinhardtii* (CC125) stock was purchased from the Chlamydomonas Resource Center at the University of Minnesota. The cells were grown in either $^{15}$N-labeled or unlabeled TAP medium at 27 °C while rotated at 80 RPM in an orbital shaker incubator (MaxQ400, Thermo Scientific, Waltham, MA). Two LED light bulbs (daylight white, 6 W and 10 W), producing ~100 $\mu mol \cdot m^{-2} sec^{-1}$ intensity radiation, were installed above the culture. A digital timer provided automated 12 h light/12 h dark cycles. Illumination was monitored using a photosynthetic active radiation (PAR) meter (Sun System, Sunlight Supply Inc., Vancouver, WA). In order to determine growth rates, cells were counted by a hemocytometer (Bright-Line, Horsham, PA).

### 2.4. Pulse-chase analysis

The experiment started with the pulse phase, in which cells were grown for 96 h in $^{15}$N-labeled TAP medium, allowing nitrogen assimilation to label the cells. In the pulse phase high fractional enrichment, $^{15}N/(^{15}N+^{14}N)$, was observed for both chlorophyll *a* (94.6%) and chlorophyll *b* (91.5%), whereas pheophytin *a* was observed at a lower percent (78.4%). Cells were then pelleted by centrifugation at 2000× *g* for 1 min, washed and re-suspended in unlabeled medium, marking the beginning of the chase phase. Sampling at several time points in the chase phase was performed by collecting ~$10^6$ cells and adjusting the volumes to 1.0 mL. These

* Corresponding author.
*E-mail address:* vertes@gwu.edu (A. Vertes).

samples were centrifuged for 1 min at 5000× *g* to produce pellets, which were then re-spun for 1 min at 2000× *g* in an EconoSpin silica membrane (1 μm pore size) cartridge held within a spin tube (Epoch Biolabs, Missouri City, TX). The samples on the silica membrane were immediately frozen in the vapor of liquid nitrogen and stored at −80 °C until LAESI-IMS-MS analysis. All samples were measured on the same day to reduce instrument variability.

### 2.5. LAESI-IMS-MS analysis

A homebuilt LAESI ion source was used as described elsewhere in detail [19]. Briefly, a Nd:YAG laser pumped optical parametric oscillator (Opolette 100, Opotek, Carlsbad, CA) tuned to 2.94 μm wavelength delivered 5 ns laser pulses with 20 Hz repetition rate. The pulsed laser beam was focused through a 75 mm focal length plano-convex ZnSe lens (Infrared Optical Products, Farmingdale, NY) directly onto the frozen *C. reinhardtii* cell pellet on the silica filter. A homebuilt Peltier stage regulated to ~0 °C was used to prevent rapid melting of the pellet.

The ablation plume was intercepted by an orthogonal electrospray produced from a solution of 50% methanol containing 0.1% acetic acid. The stainless steel emitter (MT320-50-5-5, New Objective, Woburn, MA), was kept at +3300 V by a regulated power supply (PS350, Stanford Research Systems, Sunnyvale, CA). The electrospray solution was dispensed at 500 nL/min using a syringe pump (Physio 22, Harvard Apparatus, Holliston. MA). The produced ions were then detected by a high performance quadrupole time-of-flight mass spectrometer (Synapt G2S, Waters, Milford, MA). A commercial traveling-wave ion mobility system with a resolving power of $\Omega/\Delta\Omega \approx 30$ was used for IMS analysis [30]. For all experiments, the nitrogen drift gas was supplied at 90 mL/min and 3.35 mbar, and the wave height was set to 40 V, the wave velocity was held at 650 m/s, and a delay coefficient of 1.41 V was set.

### 2.6. Data processing

Isotopologs appeared as doublets in the difference heat plot under $^{15}$N-labeled or partially labeled conditions. Tentative peak assignments were based on accurate mass measurements, molecular formulas derived from accurate mass, (ChemCalc), database searches (Plant Metabolic Network, Lipids Maps, IsoMETLIN, and Mascot) and previous experiments [21]. The DriftScope 2.4 utility was used to visualize the DT vs. *m/z* plots and the HDMS Compare software (Version 1.0, Waters, Milford, MA) produced the heat plots, showing differences between two DT vs. *m/z* plots. Collision cross sections (CCS) for the detected ions were derived using polyalanine based calibration with repeat units between n = 4 and n = 14, covering the *m/z* region from 233 to 943, as discussed elsewhere in detail [20]. Spectral overlaps due to the natural $^{13}$C isotope peaks were deconvoluted to obtain the proper intensities of labeled and unlabeled compounds. To estimate the number of components, including structural isomers and conformers, detected using LAESI-IMS-MS, all the peaks were found within the DT vs. *m/z* plot. The mass spectrum integrated over DT was processed for deisotoping (mMass 3), followed by manual subtraction of the $Na^+$ and $K^+$ adducts and estimation of the structural isomers and conformers based on the number of isobaric peaks in the DT vs. *m/z* plot [31].

## 3. Results and discussion

Within a typical positive ion mode LAESI-IMS-MS experiment sampling alga cells, the DT vs. *m/z* plot contained ~6000 features, including isotope peaks, quasi-molecular ions, i.e., sodium and/or potassium adducts, structural isomers and conformers with distinct CCSs. Integrating overall the DTs resulted in a mass spectrum with 637 features that was reduced to 392 peaks after deisotoping. After subtracting the 54 $Na^+$ and 46 $K^+$ adducts, 292 peaks were left. Revisiting the DT vs. *m/z* plot enabled us to estimate the number of structural isomers and conformers as ~1760 resulting in a final count of ~2052 detected components, of which ~980 were lipids. Most of the detected components were not identified by tandem MS.

### 3.1. Stable isotope labeling of microalgae in combination with LAESI-IMS

The effect of stable isotope labeling on the cell growth was explored. *C. reinhardtii* cells were cultured in $^{15}$N-labeled and in unlabeled media. After acclimating the cultures for ten generations (i.e., for 240 h), growth rates were measured. Both cultures exhibited similar growth rates during 72 h (Fig. 1a) without significant differences in cell morphology (Fig. 1b). Apart from the presence of isotopologs, similar spectral features were observed for the two cultures (Fig. 1c). The mass difference of the isotopologs revealed the number of nitrogen atoms in the molecule. For example, chlorophyll *b* was present as *m/z* 907.521 in the unlabeled medium, whereas it was detected as *m/z* 911.512 in the $^{15}$N-TAP medium, indicating the presence of four nitrogen atoms.

Lipid isotopologs that contain one nitrogen atom, such as diacylglyceryl N,N,N-trimethylhomoserines (DGTS) were also detected. Identification of the acyl chain lengths and verification of the $^{15}$N incorporation was achieved by tandem MS (Fig. S1). Briefly, the ion assigned as DGTS(16:0/18:3) in the $^{15}$N medium had a nominal *m/z* 735 and the related lyso-lipid fragments appeared at *m/z* 497 and 475, and the trimethylserine head group was detected at *m/z* 237. In the unlabeled medium the corresponding isotopolog ions were

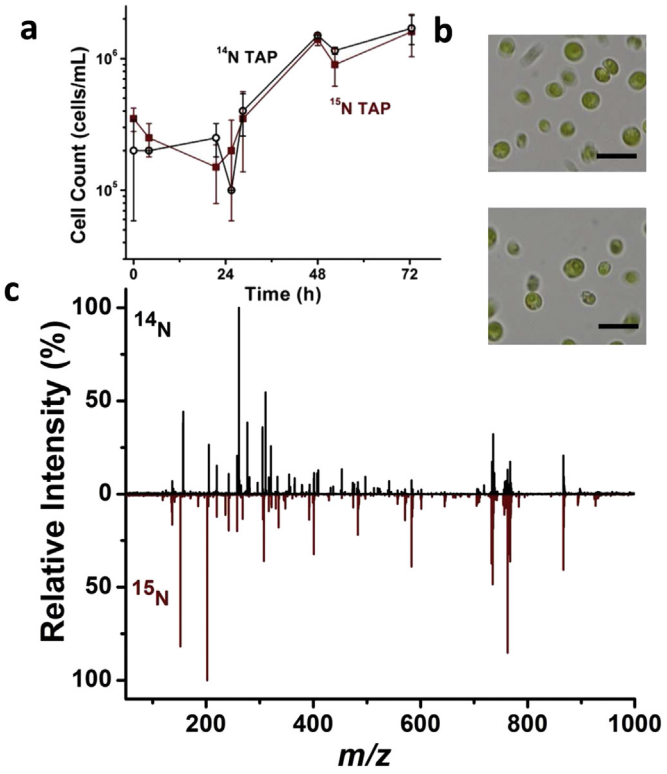


**Fig. 1.** (a) Cell growth rates are not affected by $^{15}$N isotope labeling of medium. (b) Bright field microscope image of *C. reinhardtii* cultured in (top) TAP and (bottom) $^{15}$N-TAP show no differences. Scale bar is 100 μm. (c) Representative LAESI mass spectra of *C. reinhardtii* pellet cultured in (top) unlabeled and (bottom) $^{15}$N-labeled TAP media.

present at nominal *m/z* 734, 496, 474 and 236, respectively. Other compounds, such as chlorophyll *a*, showed similar behavior regarding isotope assimilation (Fig. S1).

### 3.2. Enhanced analysis of isotopologs by IMS

Isotope substitution has negligible effect on the size and shape of an ion resulting in indistinguishable CCS values for isotopologs. The CCS in combination with accurate *m/z* and the fragmentation pattern in tandem MS provide increased confidence in the identifications of chemical species. The isotopologs of metabolites (Fig. 2a), lipids (Fig. 2b), and peptides (Fig. 2c) were investigated by pulse-chase analysis. For example two similar DGTS lipid ions were compared. The lipid DGTS(18:4/16:0) containing $^{14}N$ at a nominal *m/z* of 732 and the $^{15}N$ labeled version at 733 had identical drift time (DT) ranges between 153 and 160 m s (CCS of 291.5 ± 1.9 Å$^2$). Likewise, DGTS(18:3/16:0) at a nominal *m/z* of 734 and 735 corresponding to $^{14}N$ and $^{15}N$, respectively, exhibited DT ranges between 155 and 162 m s (corresponding to CCS = 293.8 ± 1.9 Å$^2$). Having IMS separation also helped to deconvolute the contributions of the two lipids to the natural $^{13}C$ isotope ion distribution patterns. For example selecting DT = 153 m s (see Fig. 2b), only the DGTS(18:4/16:0) isotopologs were observed, whereas DT = 162 m s only showed the DGTS(18:3/16:0) isotopologs.

Additional benefits can be derived for low intensity isotopolog ions. For example, chlorophyll *a* was observed to have a unique DT range of 178–183 ms (CCS = 314.9 ± 2.3 Å$^2$) (Fig. 2a). Here the signal-to-noise ratio of the weak ion signal associated with chlorophyll *a* was enhanced by IMS and the resulting natural $^{13}C$ isotope ion distribution patterns were clearly separated. Other chemical species, including peptides, showed unique DT and CCS values (see Table S1).

For each chase time point, ion intensities were recorded as a function of DT and *m/z*. Each of these large datasets, visualized as DT vs. *m/z* plots, contained hundreds of spectral features (see Fig. S2). Many times, low intensity isotopologs were obscured by adjacent ions of higher abundance. To recognize the isotopologs of a given compound, a difference heat plot was constructed by subtracting two DT vs. *m/z* plots (Fig. 2d) corresponding to the unlabeled and fully labeled states (see Fig. S2). Here doublets that appeared within the same DT range were indicative of isotopologs (see the framed regions in Fig. 2d). The difference between the two DT vs. *m/z* plots, with the intensities in the spectrum for the unlabeled state in red (on a scale from 0 to −100) and the labeled state in blue (on a scale from 0 to +100) accentuated the presence of isotopologs, as most of the other spectral features were canceled. Constructing the difference heat plot facilitates finding the isotopologs for a complex biological system. Zoomed regions for lyso-DGTS(18:4) and lyso-DGTS(18:3) lipids, chlorophyll *a*, DGTS(18:3/16:0) and DGTS(18:4/16:0), and a 2.8 kDa peptide showed isotopologs with mass shifts corresponding to the number of nitrogen atoms in these molecules. This heat plot can be further analyzed for doublets to identify other isotopolog pairs including lower mass metabolites that are harder to detect due to spectral interferences.

### 3.3. Turnover of biomolecules

#### 3.3.1. Lipid turnover rates in algae

Studying the biosynthesis of lipids is motivated by their diverse biological functions, such as forming membranes, acting as signaling molecules, and serving as energy storage compounds. Isotope incorporation and lipid turnover in some cultured cells has been followed by radioactive tracers and/or pulse-chase analysis [27,32]. Due to the large diversity of lipids in recent metabolic network reconstructions (e.g., 370 lipid species and 688 associated reactions in the iRC1080 reconstruction) and the large variety of microbial strains, high throughput methods are needed to measure turnover rates [3].

To explore the turnover rates of nitrogen containing lipids in

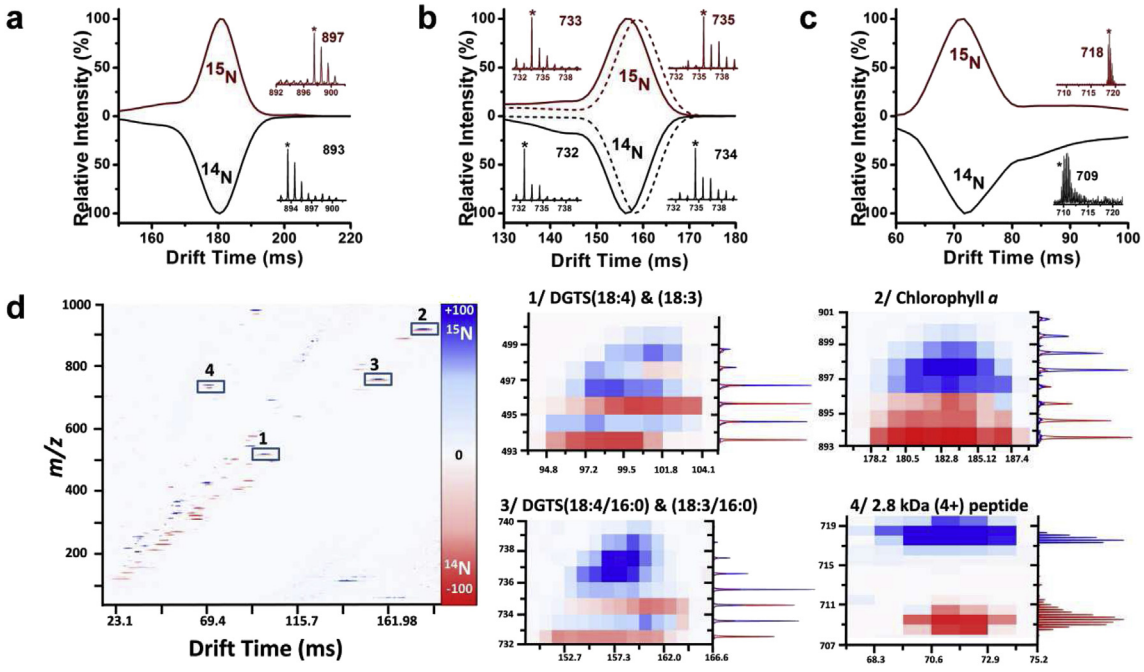


**Fig. 2.** The DT distribution plot for isotopologs from *C. reinhardtii* cells cultured in $^{15}N$ (top) and $^{14}N$ (bottom) media for (a) chlorophyll *a*, for (b) two DGTS lipids DGTS (18:4/16:0) and DGTS (18:3/16:0) and for (c) a 2.8 kDa peptide. (d) Difference heat plot, reveals the intensity differences between the ions from cells cultured in $^{15}N$ (blue) and $^{14}N$ (red) media. Zoomed regions (right) show doublets of isotopologs for two lyso-DGTS, chlorophyll *a*, two DGTS lipids, and a peptide with the corresponding mass spectra to the right. (For interpretation of the references to colour in this figure caption, the reader is referred to the web version of this article.)

*C. reinhardtii*, we focused on the DGTS and lyso-DGTS species, lipids predominantly found in plants and algae. For example, combined isotope distributions derived from the presence of natural $^{13}C$ and the introduced $^{15}N$ label for the DGTS(18:4/16:0) and DGTS(18:3/16:0) molecular ions were monitored in the chase phase for 72 h (see Fig. 3). In this somewhat complex case, typical of lipids with differing only in the presence of an additional double bond, the isotope distribution pattern for the less saturated species is a convolution of contributions from $^{13}C$, $^{15}N$ and the more saturated species. In Fig. 3, at the start of the chase phase (0 h) only $^{15}N$ labeled lipid species were present shown in gray and red. As time progressed, the microalgae incorporated the unlabeled molecules from the medium resulting in the presence of the unlabeled forms of the two lipids, shown in green and blue. At 72 h, the labeled DGTS(18:3/16:0) (shown in red) completely turned over and only the unlabeled form (blue) was detected. In contrast, the lipid DGTS(18:4/16:0) was still detected in both labeled (gray) and unlabeled (green) forms. To obtain the undistorted intensities associated with $^{15}N$ labeling, the contributions from $^{13}C$ and less saturated form of the lipid had to be subtracted.

Following the deconvoluted fractional enrichment, $^{15}N/(^{14}N+^{15}N)$, as a function of time over a 72 h time period, the turnover for six lyso-DGTS and six DGTS lipid species were determined (Fig. S3). The intensity ratios for the turnover of these lipids followed first-order kinetics (Fig. S4). Overall the turnover rates ranged between $(1.25 \pm 0.05) \times 10^{-2}$ $h^{-1}$ and $(2.56 \pm 0.27) \times 10^{-2}$ $h^{-1}$, and the corresponding half-lives were between 55.5 ± 2.3 and 27.1 ± 2.9 h (see Table 1).

**Table 1**
Turnover rates and half-lives of lipids in *C. reinhardtii*.

| Lipid | k ($h^{-1}$) | $t_{1/2}$ (h) |
|---|---|---|
| Lyso-DGTS(16:0) | $1.59 \pm 0.2 \times 10^{-2}$ | 43.6 ± 4.5 |
| Lyso-DGTS(16:2) | $1.99 \pm 0.05 \times 10^{-2}$ | 34.8 ± 0.9 |
| Lyso-DGTS(16:4) | $2.56 \pm 0.3 \times 10^{-2}$ | 27.1 ± 2.9 |
| Lyso-DGTS(18:3) | $1.73 \pm 0.1 \times 10^{-2}$ | 40.0 ± 2.5 |
| Lyso-DGTS(18:4) | $1.40 \pm 0.1 \times 10^{-2}$ | 49.5 ± 4.1 |
| DGTS(16:1/16:0) | $1.48 \pm 0.2 \times 10^{-2}$ | 46.9 ± 4.4 |
| DGTS(16:2/16:0) | $1.72 \pm 0.1 \times 10^{-2}$ | 40.2 ± 3.9 |
| DGTS(16:3/16:0) | $1.54 \pm 0.2 \times 10^{-2}$ | 44.9 ± 7.1 |
| DGTS(18:3/16:0) | $1.45 \pm 0.05 \times 10^{-2}$ | 47.6 ± 2.2 |
| DGTS(18:4/16:0) | $1.25 \pm 0.05 \times 10^{-2}$ | 55.5 ± 2.3 |

### 3.3.2. Porphyrin turnover rates

Photosynthesis is an extensively studied cellular function due to its importance in the large scale conversion of light to biochemical energy [33,34]. Biosynthesis of chlorophyll *a* occurs through the chlorophyll cycle and two alternative pathways from chlorophyllide *a*. Its degradation reactions lead back to chlorophyllide *a*, and to pheophytin *a*. In unicellular and centric diatom microalgae, perturbation of the chlorophyll cycle by $^{15}N$ and $^{18}O$ stable isotopes showed a wide range of species dependent half-lives for chlorophyll *a* ranging from 30 min to many days [32,35–37]. Studying the chlorophyll cycle for different genetic variants under a variety of environmental conditions would require a large set of lengthy experiments.

We used the high throughput LAESI-IMS-MS technique to determine the turnover rates of three porphyrin compounds within the chlorophyll cycle; chlorophyll *a*, chlorophyll *b*, and pheophytin *a*.

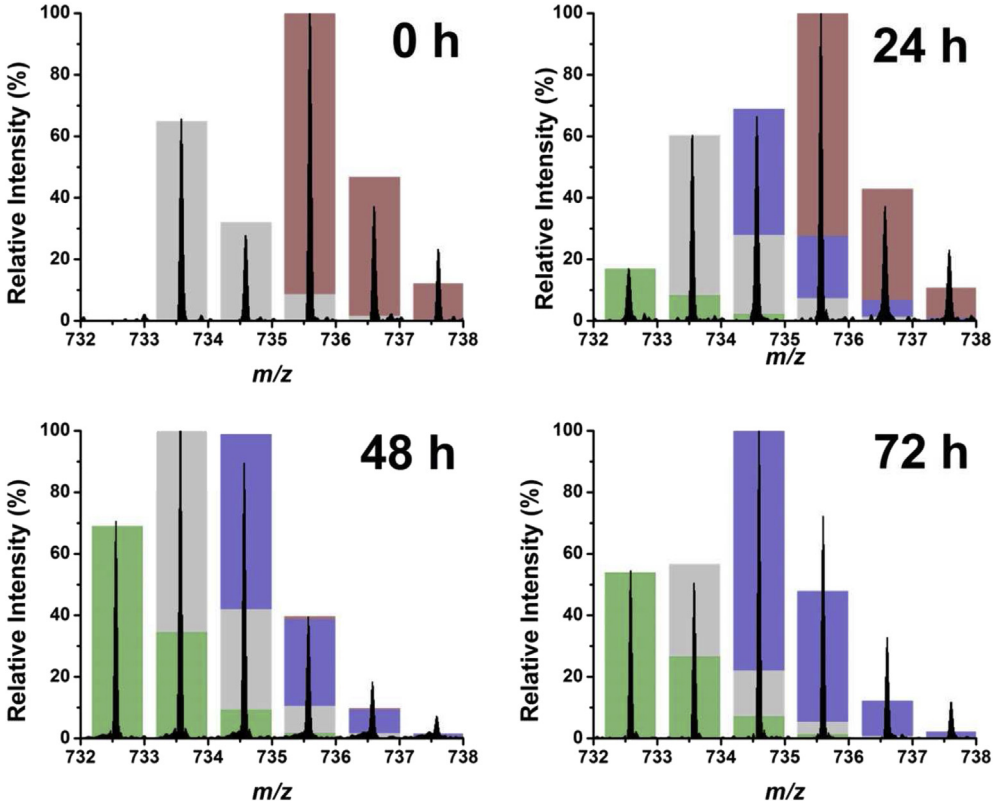


**Fig. 3.** Isotope distribution patterns in pulse-chase analysis of DGTS (18:4/16:0) and DGTS (18:3/16:0) lipid species followed over a 72 h period. Black traces correspond to experimental spectra, whereas color coded bars show calculated contributions of natural $^{13}C$ and introduced $^{15}N$ isotopologs. Green and blue represent the $^{14}N$ isotopologs of DGTS (18:4/16:0) and DGTS (18:3/16:0), respectively, whereas gray and red correspond to their $^{15}N$ counterparts. (For interpretation of the references to colour in this figure caption, the reader is referred to the web version of this article.)

During a 72 h pulse-chase experiment (Fig. S5) these compounds and their isotopologs were detected and quantitated at multiple time points. The identification of these compounds were affirmed by tandem MS (Fig. S1).

It has been shown that under acidic conditions the chelating magnesium can be released in porphyrins [38]. Due to the acidity of the electrospray solution in LAESI, this can result in the formation of pheophytin *a* from chlorophyll *a* and skew the measurements. To verify that the detected pheophytin *a* was entirely the result of biological processes, chlorophyll *a* standard was studied by LAESI-IMS-MS. The results showed that only 3.5 ± 1.2% of pheophtyin *a* was formed due to the acidic electrospray conditions. This represented a negligible correction to our kinetics studies.

To obtain kinetic information, the fractional enrichments were plotted as a function of time (Fig. 4a) and for all three compounds, chlorophyll *a* ($R^2$ = 0.998), chlorophyll *b* ($R^2$ = 0.997), and pheophytin *a* ($R^2$ = 0.980), they followed first-order kinetics (Fig. 4b). The turnover rate rates of chlorophyll *a*, chlorophyll *b*, and pheophytin *a* were 2.88 ± 0.3 × $10^{-2}$ $h^{-1}$, 1.55 ± 0.05 × $10^{-2}$ $h^{-1}$, and 3.68 ± 0.5 × $10^{-2}$ $h^{-1}$, respectively. Half-lives were calculated to be 24.1 ± 2.2 h for chlorophyll *a*, 44.7 ± 1.6 h for chlorophyll *b*, and 18.9 ± 2.7 h for pheophytin *b*. It was observed that pheophytin *a* turned over ~2.4 times faster then chlorophyll *b* and ~1.3 times faster than chlorophyll *a*.

### 3.3.3. Large molecule turnover analysis

Among the detected peptides from the *C. reinhardtii* samples, quadruply charged ions at nominal *m/z* 709 were selected for the demonstration of pulse-chase analysis. Upon $^{15}N$ enrichment, the *m/z* 709 peak shifted to *m/z* 718 indicating the presence of 36 exchangeable nitrogen atoms (Fig. S6a). The molecular mass of the unlabeled isotopolog calculated by the Maxent 3 algorithm was 2835.98 ± 1.56 Da. The observed isotopologs in the +4 charge state had the same CCS = 753.9 ± 5.8 $Å^2$ cross section values. This peptide was also detected in the +3 charge state with CCS = 660.5 ± 5.4 $Å^2$.

The half-lives determined based on the two charge states, 10.9 ± 4.1 h and 9.9 ± 5.8 h for the +4 and + 3 ions, respectively, were very similar (Fig. S6c), yielding an overall peptide half-life of 10.4 ± 3.6 h.

In addition to metabolites and lipids, pulse chase analysis in combination with LAESI-IMS-MS was also used to follow the turnover of biopolymers, i.e., peptides, in the same experiment. Conventional proteomics analysis requires extraction, purification, and chromatographic separation that can take in excess of 100 min for every sample [39]. The benefit of LAESI-IMS-MS is that both abundant and low level components can be detected from the same sample simultaneously within ~5 min.

## 4. Conclusions

The integration of pulse-chase analysis with LAESI-IMS-MS can provide rapid assessment of metabolite, lipid, and peptide turnover rates in microorganisms, plants, and animals. Identification of isotopologs in pulse-chase analysis experiments is simplified by the construction of difference heat plots in the DT vs. *m/z* space. Once the isotopologs appearing as doublets are pinpointed, the turnover rates are determined from the chase phase kinetics. This LAESI-IMS-MS based strategy can be applied to a wide variety of biological systems without the need to develop sample specific extraction protocols. Future applications are expected in metabolomics research, drug metabolism studies and metabolic engineering.

## Acknowledgments

This material is based upon work supported by the U.S. Department of Energy, Office of Science, Office of Basic Energy Sciences, Chemical Sciences, Geosciences and Biosciences Division under Award Number DE-FG02-01ER15129 to A.V., and the grant ANR-Biomass-BioEnergies-DiaDomOil to D.F.

## Appendix A. Supplementary data

Supplementary data related to this article can be found at http://dx.doi.org/10.1016/j.aca.2015.08.047.

## References

[1] R.L. Chang, L. Ghamsari, A. Manichaikul, E.F.Y. Hom, S. Balaji, W. Fu, Y. Shen, T. Hao, B.O. Palsson, K. Salehi-Ashtiani, J.A. Papin, Metabolic network reconstruction of *Chlamydomonas* offers insight into light-driven algal metabolism, Mol. Syst. Biol. 7 (2011).
[2] D.J. Creek, A. Chokkathukalam, A. Jankevics, K.E.V. Burgess, R. Breitling, M.P. Barrett, Stable isotope-assisted metabolomics for network-wide metabolic pathway elucidation, Anal. Chem. 84 (2012) 8442–8447.
[3] A. Chokkathukalam, D.-H. Kim, M.P. Barrett, R. Breitling, D.J. Creek, Stable isotope-labeling studies in metabolomics: new insights into structure and dynamics of metabolic networks, Bioanalysis 6 (2014) 511–524.
[4] M.L. Reaves, B.D. Young, A.M. Hosios, Y.-F. Xu, J.D. Rabinowitz, Pyrimidine homeostasis is accomplished by directed overflow metabolism, Nature 500 (2013) 237-+.
[5] W. Wiechert, C-13 metabolic flux analysis, Metab. Eng. 3 (2001) 195–206.
[6] P.K. Ajikumar, W.-H. Xiao, K.E.J. Tyo, Y. Wang, F. Simeon, E. Leonard, O. Mucha, T.H. Phon, B. Pfeifer, G. Stephanopoulos, Isoprenoid pathway optimization for taxol precursor overproduction in *Escherichia coli*, Science 330 (2010) 70–74.
[7] S.-E. Ong, M. Mann, A practical recipe for stable isotope labeling by amino acids in cell culture (SILAC), Nat. Protoc. 1 (2006) 2650–2660.
[8] T.P. Conrads, K. Alving, T.D. Veenstra, M.E. Belov, G.A. Anderson, D.J. Anderson, M.S. Lipton, L. Pasa-Tolic, H.R. Udseth, W.B. Chrisler, B.D. Thrall, R.D. Smith, Quantitative analysis of bacterial and mammalian proteomes using a combination of cysteine affinity tags and N-15-metabolic labeling, Anal. Chem. 73 (2001) 2132–2139.
[9] L. Pasa-Tolic, P.K. Jensen, G.A. Anderson, M.S. Lipton, K.K. Peden, S. Martinovic, N. Tolic, J.E. Bruce, R.D. Smith, High throughput proteome-wide precision measurements of protein expression using mass spectrometry, J. Am. Chem. Soc. 121 (1999) 7949–7950.
[10] M.P. Washburn, R. Ulaszek, C. Deciu, D.M. Schieltz, J.R. Yates, Analysis of quantitative proteomic data generated via multidimensional protein identification technology, Anal. Chem. 74 (2002) 1650–1657.
[11] C.J. Nelson, E.L. Huttlin, A.D. Hegeman, A.C. Harms, M.R. Sussman, Implications of N-15-metabolic labeling for automated peptide identification in *Arabidopsis thaliana*, Proteomics 7 (2007) 1279–1292.
[12] A. Lafaye, J. Labarre, J.C. Tabet, E. Ezan, C. Junot, Liquid chromatography – mass spectrometry and N-15 metabolic labeling for quantitative metabolic profiling, Anal. Chem. 77 (2005) 2026–2033.
[13] J. Krijgsveld, R.F. Ketting, T. Mahmoudi, J. Johansen, M. Artal-Sanz, C.P. Verrijzer, R.H.A. Plasterk, A.J.R. Heck, Metabolic labeling of C-elegans and D-melanogaster for quantitative proteomics, Nat. Biotechnol. 21 (2003) 927–931.
[14] J.M. Reiner, The study of metabolic turnover rates by means of isotopic tracers. I. Fundamental relations, Arch. Biochem. Biophys. 46 (1953) 53–79.
[15] G. Mastrobuoni, S. Irgang, M. Pietzke, H.E. Assmus, M. Wenzel, W.X. Schulze, S. Kempa, Proteome dynamics and early salt stress response of the photosynthetic organism *Chlamydomonas reinhardtii*, BMC Genom. 13 (2012).
[16] E. Fischer, U. Sauer, Metabolic flux profiling of *Escherichia coli* mutants in central carbon metabolism using GC-MS, Eur. J. Biochem. 270 (2003) 880–891.
[17] R.G. Ratcliffe, Y. Shachar-Hill, Measuring multiple fluxes through plant metabolic networks, Plant J. 45 (2006) 490–511.
[18] U. Sauer, High-throughput phenomics: experimental methods for mapping fluxomes, Curr. Opin. Biotechnol. 15 (2004) 58–63.
[19] P. Nemes, A. Vertes, Laser ablation electrospray ionization for atmospheric pressure, in vivo, and imaging mass spectrometry, Anal. Chem. 79 (2007) 8098–8106.
[20] B. Shrestha, A. Vertes, High-throughput cell and tissue analysis with enhanced molecular coverage by laser ablation electrospray ionization mass spectrometry using ion mobility separation, Anal. Chem. 86 (2014) 4308–4315.
[21] S.A. Stopka, B. Shrestha, E. Marechal, D. Falconet, A. Vertes, Metabolic transformation of microalgae due to light acclimation and genetic modifications followed by laser ablation electrospray ionization mass spectrometry with ion mobility separation, Analyst 139 (2014) 5946–5954.
[22] E.H. Harris, *Chlamydomonas* as a model organism, Annu. Rev. Plant Physiol. Plant Mol. Biol. 52 (2001) 363–406.

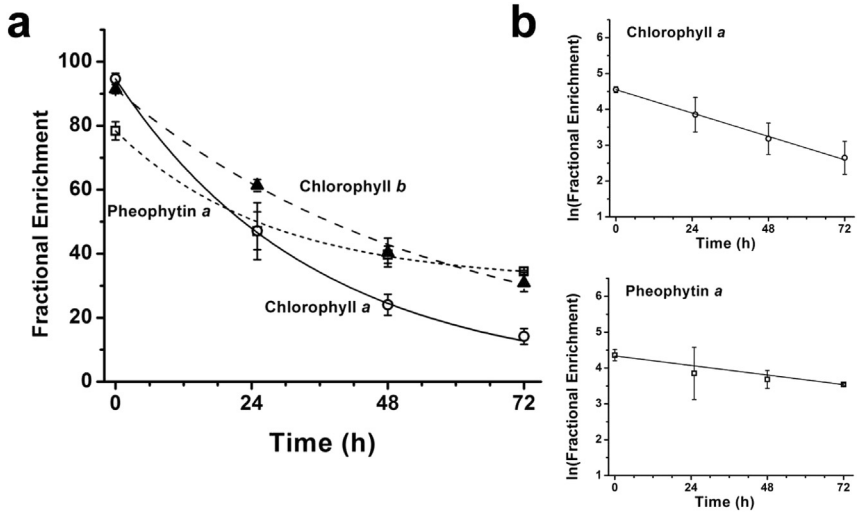


**Fig. 4.** (a) Kinetics of N isotope exchange in pheophytin *a* (□), chlorophyll *b* (▲), and chlorophyll *a* (○) over a 72 h period. (b) Fractional enrichment follows first order kinetics for (top) chlorophyll *a* and (bottom) pheophytin *a*.


[23] C. Bolling, O. Fiehn, Metabolite profiling of *Chlamydomonas reinhardtii* under nutrient deprivation, Plant Physiol. 139 (2005) 1995–2005.
[24] H. Heide, A. Nordhues, F. Drepper, S. Nick, M. Schulz-Raffelt, W. Haehnel, M. Schroda, Application of quantitative immunoprecipitation combined with knockdown and cross-linking to *Chlamydomonas* reveals the presence of vesicle-inducing protein in plastids 1 in a common complex with chloroplast HSP90C, Proteomics 9 (2009) 3079–3089.
[25] A. Gruhler, W.X. Schulze, R. Matthiesen, M. Mann, O.N. Jensen, Stable isotope labeling of *Arabidopsis thaliana* cells and quantitative proteomics by mass spectrometry, Mol. Cell. Proteomics 4 (2005) 1697–1709.
[26] D. Lewandowska, S. ten Have, K. Hodge, V. Tillemans, A.I. Lamond, J.W.S. Brown, Plant SILAC: stable-isotope labelling with amino acids of *Arabidopsis* seedlings for quantitative proteomics, PLoS One 8 (2013).
[27] B. Naumann, A. Busch, J. Allmer, E. Ostendorf, M. Zeller, H. Kirchhoff, M. Hippler, Comparative quantitative proteomics to investigate the remodeling of bioenergetic pathways under iron deficiency in *Chlamydomonas reinhardtii*, Proteomics 7 (2007) 3964–3979.
[28] M.-L.A. Sauer, B. Xu, F. Sutton, Metabolic labeling with stable isotope nitrogen (N-15) to follow amino acid and protein turnover of three plastid proteins in *Chlamydomonas reinhardtii*, Proteome Sci. 12 (2014).
[29] D.S. Gorman, R.P. Levine, Cytochrome f and plastocyanin: their sequence in the photosynthetic electron transport chain of *Chlamydomonas reinhardi*, Proc. Natl. Acad. Sci. U. S. A. 54 (1965) 1665–1669.
[30] K. Giles, J.P. Williams, I. Campuzano, Enhancements in travelling wave ion mobility resolution, Rapid Commun. Mass Spectrom. 25 (2011) 1559–1566.
[31] M. Strohalm, D. Kavan, P. Novak, M. Volny, V. Havlicek, mMass 3: a cross-platform software environment for precise analysis of mass spectrometric data, Anal. Chem. 82 (2010) 4648–4651.
[32] M. Schliep, B. Crossett, R.D. Willows, M. Chen, O-18 labeling of chlorophyll d in acaryochloris marina reveals that chlorophyll a and molecular oxygen are precursors, J. Biol. Chem. 285 (2010) 28450–28456.
[33] H. Thomas, Tansley review no 92-chlorophyll: a symptom and a regulator of plastid development, New Phytol. 136 (1997) 163–181.
[34] D. Vavilin, W. Vermaas, Continuous chlorophyll degradation accompanied by chlorophyllide and phytol reutilization for chlorophyll synthesis in *Synechocystis* sp PCC 6803, Biochim. Biophys. Acta Bioenerg. 1767 (2007) 920–929.
[35] D. Vavilin, D.C. Brune, W. Vermaas, N-15-labeling to detennine chlorophyll synthesis and degradation in *Synechocystis* sp PCC 6803 strains lacking one or both photosystems, Biochim. Biophys. Acta Bioenerg. 1708 (2005) 91–101.
[36] K.H. Grumbach, H.K. Lichtenthaler, K.H. Erismann, Incorporation of CO-14(2) in photosynthetic pigments of chlorella-pyrenoidosa, Planta 140 (1978) 37–43.
[37] R. Goericke, N.A. Welschmeyer, Pigment Turnover in the marine diatom thalassiosira-weissflogii .1. The 14CO2-labeling kinteics of chlorophyll-A, J. Phycol. 28 (1992) 498–507.
[38] T. Suzuki, H. Midonoya, Y. Shioi, Analysis of chlorophylls and their derivatives by matrix-assisted laser desorption/ionization-time-of-flight mass spectrometry, Anal. Biochem. 390 (2009) 57–62.
[39] T. Muehlhaus, J. Weiss, D. Hemme, F. Sommer, M. Schroda, Quantitative shotgun proteomics using a uniform n-15-labeled standard to monitor proteome dynamics in time course experiments reveals new insights into the heat stress response of *Chlamydomonas reinhardtii*, Mol. Cell. Proteomics 10 (2011).

Supporting information for

# Turnover Rates in Microorganisms by Laser Ablation Electrospray Ionization Mass Spectrometry and Pulse-chase Analysis

*Sylwia A. Stopka,[1] Tarek R. Mansour,[1] Bindesh Shrestha,[1] Éric Maréchal,[2] Denis Falconet[2] and Akos Vertes[1*]*

[1]Department of Chemistry, W. M. Keck Institute for Proteomics Technology and Applications, The George Washington University, Washington, DC 20052, USA

[2]Laboratoire de Physiologie Cellulaire et Végétale, UMR 5168, CEA-CNRS-INRA-Univ. Grenoble Alpes, Grenoble, France

*Corresponding Author: Tel.: +1 (202) 994-2717; fax: +1 (202) 994-5873. E-mail address: vertes@gwu.edu (A. Vertes). Address: Department of Chemistry, The George Washington University, 800 22-nd Street, N.W., Washington, DC 20052, USA.

**SUPPORTING FIGURES**

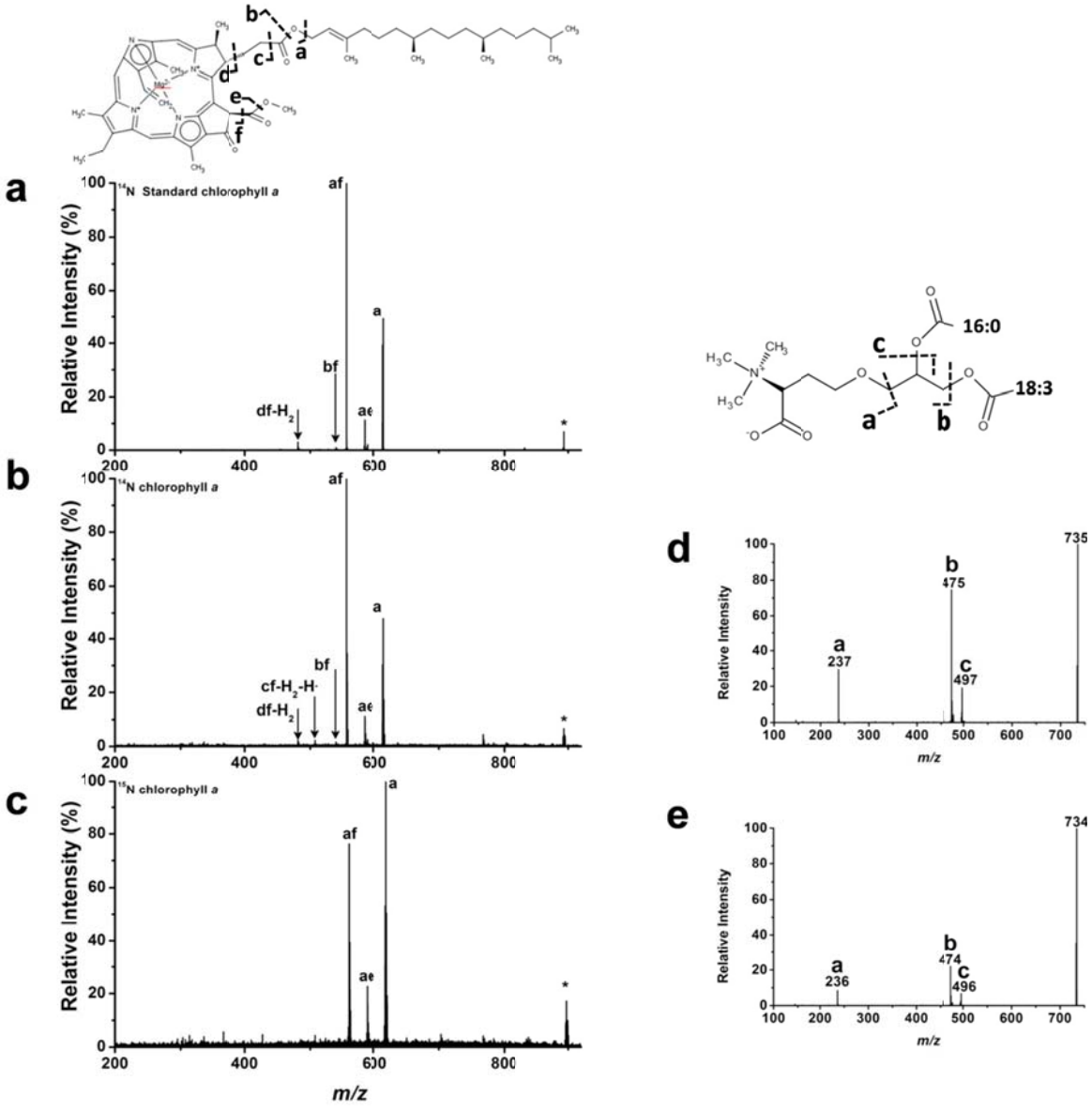


**Figure S1.** Tandem MS for isotopologs of chlorophyll *a* from (a) standard and (b and c) cell culture samples, and (d and e) DGTS(18:3/16:0) from cells. Corresponding structures and fragmentation pathways are shown in the insets.

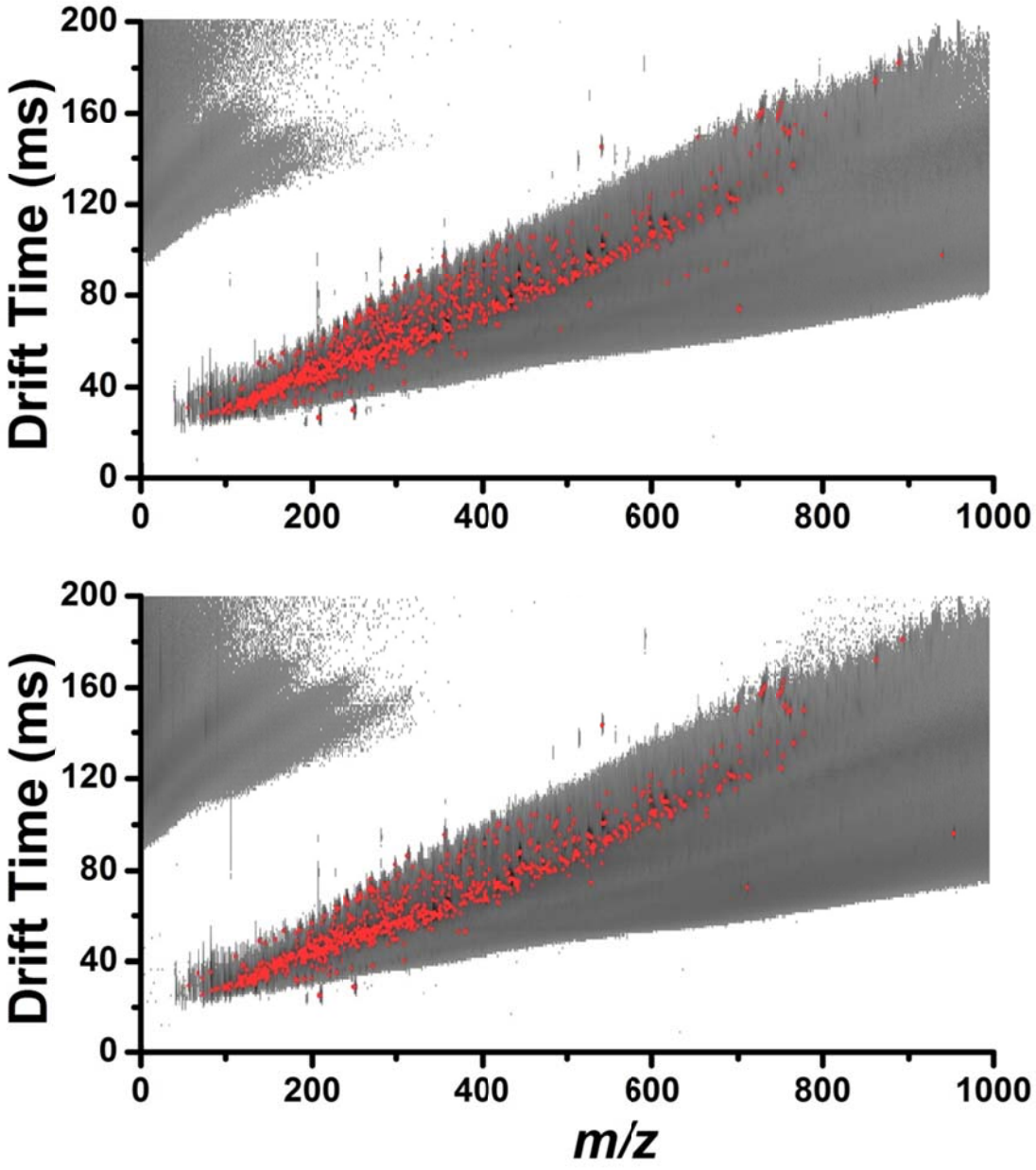


**Figure S2.** DT vs. *m/z* plots for *C. reinhardtii* cultured in (top) $^{15}$N-TAP and (bottom) $^{14}$N-TAP media.

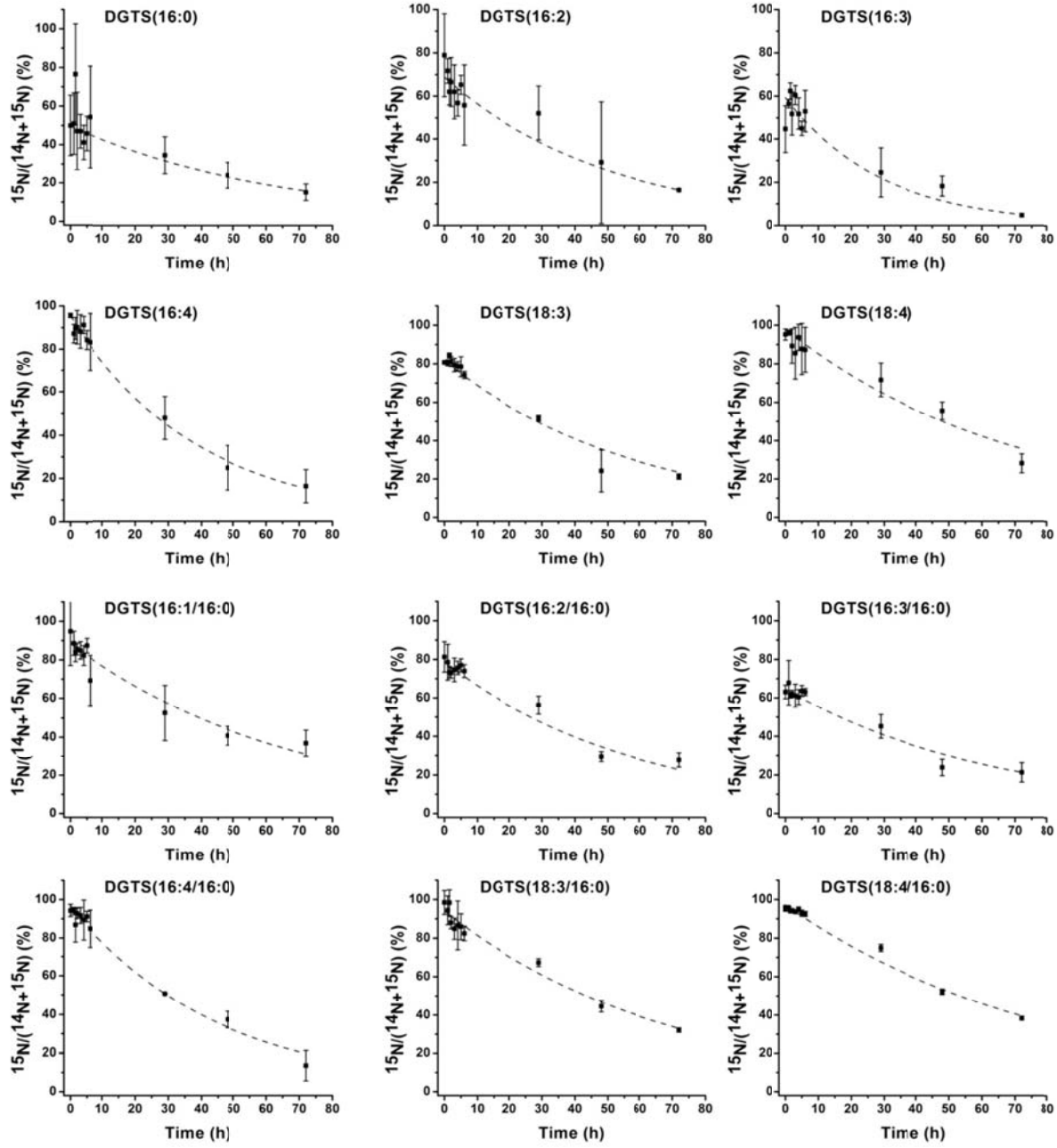


**Figure S3.** Fractional enrichment for $^{15}$N-labeled lyso-DGTS and DGTS lipids over time in the chase phase. Kinetics of the decay for all of these species exhibited a simple exponential decay.

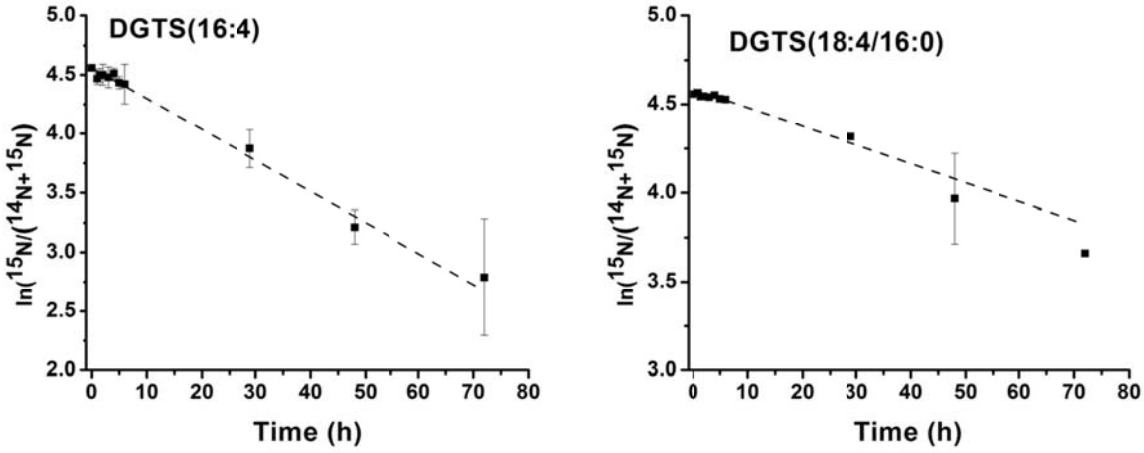


**Figure S4.** During initial 72 h of chase phase, lyso-DGTS(16:4) and DGTS(18:4/16:0) exhibited first order kinetics with regression coefficients, R, showing $R^2 = 0.97$ and $R^2 = 0.99$, respectively.

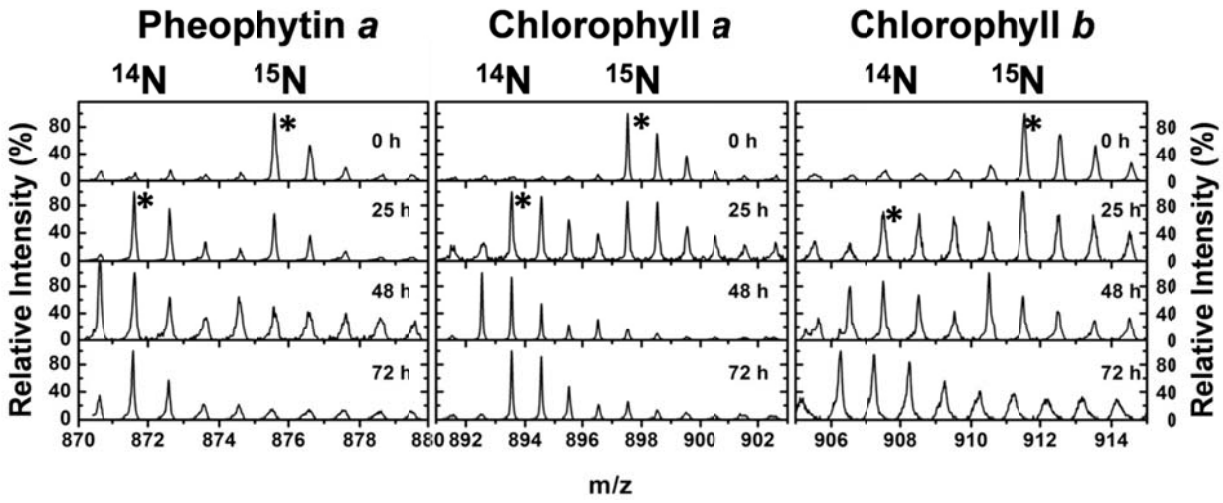


**Figure S5.** Isotope distribution changes in the LAESI mass spectra of pheophytin *a*, chlorophyll *a*, and chlorophyll *b* from *C. reinhardtii* during a 72 h pulse-chase experiment.

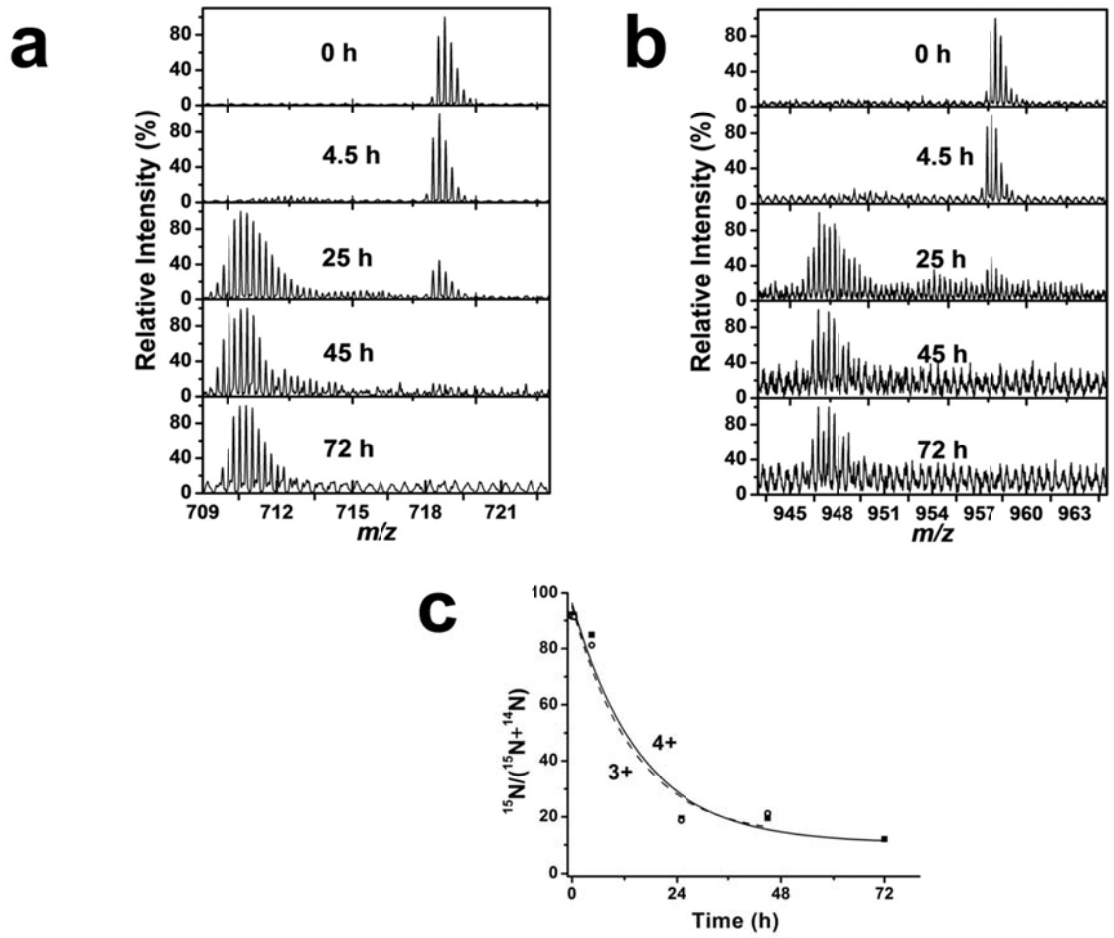


**Figure S6.** LAESI-IMS-MS spectra of **(a)** 4+ and **(b)** 3+ charge states of a 2.8 kDa peptide from *C. reinhardtii* during pulse-chase analysis followed over a 72 h time period. **(c)** Decays of fractional enrichment for the two peptide charge states follow the same kinetics.

**SUPPORTING TABLES**

**Table S1.** Collision cross sections for isotopolog ions of interest in *C. reinhardtii*. Exchanging the $^{15}N$ atoms by $^{14}N$ in the ions did not alter the corresponding CCS values.

| **Compound** | **CCS($^{14}N$) ($Å^2$) std.** | **CCS($^{14}N$) ($Å^2$)** | **CCS($^{15}N$) ($Å^2$)** |
|---|---|---|---|
| chlorophyll *a* | 314.9±2.3 | 314.9±2.3 | 314.9±2.3 |
| pheophytin *a* | 311.8±2.3 | 311.8±2.3 | 311.8±2.3 |
| chlorophyll *b* | 314.8±2.3 | 314.8±2.3 | 314.8±2.3 |
| lyso-DGTS(16:0) $H^+$ | | 230.4±0.9 | 230.4±0.9 |
| lyso-DGTS(16:2) $H^+$ | | 226.1±0.9 | 226.1±0.9 |
| lyso-DGTS(16:3) $H^+$ | | 221.7±0.8 | 221.7±0.8 |
| lyso-DGTS(16:4) $H^+$ | | 220.3±0.8 | 220.3±0.8 |
| lyso-DGTS(18:3) $H^+$ | | 231.5±0.9 | 231.5±0.9 |
| lyso-DGTS(18:4) $H^+$ | | 228.7±0.9 | 228.7±0.9 |
| DGTS (16:0/16:0) $H^+$ | | 298.5±2.0 | 298.5±2.0 |
| DGTS (16:2/16:0) $H^+$ | | 288.2±1.9 | 288.2±1.9 |
| DGTS (16:3/16:0) $H^+$ | | 285.9±1.8 | 285.9±1.8 |
| DGTS (16:4/16:0) $H^+$ | | 284.7±1.8 | 284.7±1.8 |
| DGTS(18:3/16:0) $H^+$ | | 293.8±1.9 | 293.8±1.9 |
| DGTS(18:3/16:0) $Na^+$ | | 294.8±1.9 | 294.8±1.9 |
| DGTS(18:4/16:0) $H^+$ | | 291.5±1.9 | 291.5±1.9 |
| DGTS(18:4/16:0) $Na^+$ | | 292.5±1.9 | 292.5±1.9 |
| 2.8 kDa peptide (4+) | | 753.9±5.8 | 753.9±5.8 |
| 2.8 kDa peptide (3+) | | 660.5±5.4 | 660.4±5.4 |